Q-balls in anti–de Sitter space

Arvind Rajaraman[*] and Alexander Stewart[†]
Department of Physics and Astronomy, University of California, Irvine, California 92697-4575, USA
Christopher B. Verhaaren[‡]
Department of Physics and Astronomy, Brigham Young University, Provo, Utah 84602, USA

(Received 14 December 2023; accepted 1 March 2024; published 2 April 2024)

We perform a general analysis of thin-wall Q-balls in anti–de Sitter (AdS) space. We provide numeric solutions and highly accurate analytic approximations over much of the parameter space. These analytic solutions show that AdS Q-balls exhibit significant differences from the corresponding flat-space solitons. This includes having a maximum radius beyond which the Q-balls are unstable to a new type of state where the Q-ball coexists with a gas of massive particles. The phase transition to this novel state is found to be a zero-temperature third-order transition. This, through the AdS/CFT correspondence, has implications for a scalar condensate in the boundary theory.

DOI: 10.1103/PhysRevD.109.086003

I. INTRODUCTION

The AdS/CFT correspondence [1], which relates a theory in an anti–de Sitter (AdS) space in $D+1$ dimensions with a conformal field theory in D dimensions, has been the subject of intense study for many years now. Any observable quantity in the gravitational theory (sometimes called the bulk theory) has a corresponding quantity in the boundary theory, e.g., the correlation functions of the field theory are in one-to-one correspondence with the boundary-to-boundary propagators in the bulk theory. The original correspondence of [2] has since been generalized to many other theories.

When the field theory is at nonzero temperature, it can exhibit phase transitions. In the bulk theory, these often correspond to a formation or alteration of bound states. For example, when the temperature of the field theory is increased, there is a deconfinement phase transition; this is believed to correspond to the formation of a black hole [3]. AdS can also support other solitons such as boson stars, compact objects made of scalar fields with gravitational (and potentially gauge) interactions [4–11]. These solitons exhibit yet other types of phenomena; for instance, if one considers charged boson stars, one can find a zero-temperature second-order phase transition between two types of boson stars [12].

In this work, we consider a different type of soliton in AdS. Q-balls are configurations of complex scalars ϕ that are bound together by self-interactions [13]. [Q-balls can also carry a $U(1)$ gauge charge, but here we consider Q-balls whose binding energy is dominated by the scalar attraction.] They are stable over a large range of parameter space and are hence an example of a nontopological soliton.

As Q-balls are solitons in a scalar field theory, their profiles are the solutions to a nonlinear differential equation. While this differential equation is difficult to solve exactly, extremely accurate approximation methods have been found for Q-balls with thin-wall configurations in [14]. These methods produce excellent analytic approximations to the charge and energy of both global [14] and gauged Q-balls [15] and Q-shells [16,17], as well as the radial excitations of global Q-balls [18].

Here we extend these methods to study Q-balls in AdS (some previous work on this subject is [9,19,20]). We ignore backreaction on the spacetime and hence the AdS space is taken to be a fixed background for the scalar field. We find solutions both numerically and by an extension of the methods of [14], and show excellent agreement between the approximate analytical functions and the exact numerical solutions in several different spatial dimensions. These methods agree in showing that there is generically a maximal radius for Q-balls in AdS, except for a special class of scalar potentials such as those studied in [19]. Beyond the corresponding maximal charge, we find an unexpected phase of the theory, where the Q-ball coexists with a gas of noninteracting massive particles. (A similar phenomenon has been found for Kerr black holes in AdS [21].)

[*]arajaram@uci.edu
[†]ajstewa1@uci.edu
[‡]verhaaren@physics.byu.edu

We also examine the consequences of the Q-ball physics for the dual theory on the boundary. We find an intricate phase diagram with zero-temperature phase transitions that can be either second order or, surprisingly, even third order. These high-order phase transitions are found to be generic for a large class of potentials as long as they admit Q-ball solutions. These results are seen to hold for dual theories in several dimensions.

In the next section we review the action for Q-balls in AdS and find the equations satisfied by a spherical Q-balls. We show that the thermodynamic relation $dE = \omega dQ$ between the energy and charge holds for AdS solitons. We then apply approximation techniques to find a relation between the radius of the Q-ball and the parameters of the theory in Sec. III. In Sec. IV we compare with numerical results, showing remarkable agreement for thin-wall solitons. The numerical results also confirm the analytic prediction that, unlike in flat space, there are soliton solutions with $\omega > m_\phi$. The consequences of our analytic understanding of Q-balls are further explored in Secs. V and VI with particular interest given to soliton instabilities and that, in contrast to flat space, the AdS Q-balls often have a maximum allowed radius. The implications of these results for the holographic theory on the boundary are discussed in Sec. VII. In Sec. VIII we show that the results obtained for three-dimensional AdS are easily extended to higher and lower dimensions. We close with a discussion of our results.

II. Q-BALLS IN AdS

We consider a complex scalar field propagating in a fixed AdS background. The AdS geometry is parametrized as

$$ds^2 = a(r)dt^2 - b(r)dr^2 - r^2(d\theta^2 + \sin^2\theta d\phi^2), \quad (1)$$

with

$$a(r) = 1 + \frac{r^2}{\ell^2}, \qquad b(r) = \frac{1}{1+\frac{r^2}{\ell^2}}, \quad (2)$$

where $\ell = \sqrt{-\frac{3}{\Lambda}}$ is a scale that sets the size of the AdS space.

The action for a scalar field propagating in this geometry is

$$\mathcal{S} = \int d^4x\sqrt{-g}[(\nabla_\mu\Phi)^*(\nabla^\mu\Phi) - U(\Phi\Phi^*)]. \quad (3)$$

The complex scalar field Φ is subject to a potential $U(\Phi\Phi^*)$ that preserves a global $U(1)$ symmetry and thereby leads to a conserved particle number, denoted by Q,

$$Q = i\int d^3x\sqrt{-g}(\Phi^*\partial^t\Phi - \Phi\partial^t\Phi^*). \quad (4)$$

The energy stored in the field,

$$E = \int d^3x\sqrt{-g}T^t{}_t, \quad (5)$$

is given in terms of the energy-momentum tensor

$$T_{\mu\nu} = (\nabla_\mu\Phi)^*(\nabla_\nu\Phi) + (\nabla_\nu\Phi)^*(\nabla_\mu\Phi) - g_{\mu\nu}[(\nabla_\mu\Phi)^*(\nabla^\mu\Phi) - U(\Phi\Phi^*)]. \quad (6)$$

The equation for Φ is

$$\nabla_\mu\nabla^\mu\Phi = -\frac{\partial U}{\partial\Phi^*} = -\Phi\frac{dU}{d(\Phi\Phi^*)}. \quad (7)$$

We look for spherical Q-ball solutions; this implies that we take the scalar field to be of the form

$$\Phi = \frac{\phi_0}{\sqrt{2}}f(r)e^{-i\omega t}, \quad (8)$$

where $\phi_0/\sqrt{2}$ is the value of the nontrivial minimum of $U(\Phi\Phi^*)/(\Phi\Phi^*)$. To make a connection with the typical flat-space characterization of Q-balls, we also define

$$\omega_0^2 \equiv \left.\frac{U(\Phi\Phi^*)}{\Phi\Phi^*}\right|_{\Phi=\phi_0/\sqrt{2}}. \quad (9)$$

The dimensionless function $f(r)$ is referred to as the profile of the field configuration. The equation of motion for the field can then be written as an equation to determine this profile,

$$\frac{d^2f}{dr^2} + \frac{2}{r}\frac{1+2r^2/\ell^2}{1+r^2/\ell^2}\frac{df}{dr} = \frac{f}{1+r^2/\ell^2}\left(\frac{dU}{d(\Phi\Phi^*)} - \frac{\omega^2}{1+r^2/\ell^2}\right). \quad (10)$$

Note that as $\ell\to\infty$ this becomes the usual flat-space equation for f [13].

In general, the equation for f cannot be solved analytically. In this study, following [14], we focus on a sextic potential,

$$U(|\phi|) = m_\phi^2|\phi|^2 - \beta|\phi|^4 + \frac{\xi}{m_\phi^2}|\phi|^6. \quad (11)$$

While a specific choice, this potential captures the qualities of many potentials that give rise to Q-balls [22]. In particular, we expect that any potential that gives rise to thin-wall Q-balls will have qualitatively similar results. In this potential, we have used the mass of the scalar field to

determine the estimated scaling of higher-dimension operators. Our assumption of the scalar field not backreacting on the spacetime is essentially that m_ϕ and ϕ_0 are much smaller than the Planck scale. We also assume that the cosmological constant Λ is much smaller than m_ϕ to ensure that $\ell^2|\phi|^6$ contributions to the potential are subleading. This leads to the constraint $\ell m_\phi \gg 1$.

The potential parameters given above are mapped to the Q-ball parameters ϕ_0 and ω_0 by

$$\phi_0 = m_\phi\sqrt{\frac{\beta}{\xi}}, \qquad \omega_0 = m_\phi\sqrt{1-\frac{\beta^2}{4\xi}}. \tag{12}$$

It is convenient both for numerical analyses and in determining how various quantities depend on the parameters of the theory to define the dimensionless quantities

$$\Phi_0 = \frac{\phi_0}{\sqrt{m_\phi^2-\omega_0^2}}, \qquad \Omega_{(0)} = \frac{\omega_{(0)}}{\sqrt{m_\phi^2-\omega_0^2}},$$
$$\rho = r\sqrt{m_\phi^2-\omega_0^2}, \qquad \lambda = \ell\sqrt{m_\phi^2-\omega_0^2}. \tag{13}$$

We see that our $\ell m_\phi \gg 1$ constraint becomes $\lambda \gg 1$. The f equation can then be written as

$$f'' + \frac{2}{\rho}\frac{1+2\rho^2/\lambda^2}{1+\rho^2/\lambda^2}f' = \frac{f}{1+\rho^2/\lambda^2}\left[1-\frac{\Omega^2}{1+\rho^2/\lambda^2}+\Omega_0^2-4f^2+3f^4\right], \tag{14}$$

while the charge is

$$Q = 4\pi\Phi_0^2\Omega\int_0^\infty \mathrm{d}\rho\rho^2\frac{f^2}{1+\rho^2/\lambda^2} \tag{15}$$

and the energy is

$$E = \sqrt{m_\phi^2-\omega_0^2}2\pi\Phi_0^2\int_0^\infty \mathrm{d}\rho\rho^2\left(\frac{\Omega^2 f^2}{1+\rho^2/\lambda^2}+f'^2(1+\rho^2\lambda^2) + f^2(1-f^2)^2+\Omega_0^2 f^2\right) = \omega Q - L, \tag{16}$$

where the Lagrangian is given by

$$L = \sqrt{m_\phi^2-\omega_0^2}2\pi\Phi_0^2\int_0^\infty \mathrm{d}\rho\rho^2\left(\frac{\Omega^2 f^2}{1+\rho^2/\lambda^2}-f'^2(1+\rho^2\lambda^2) - f^2(1-f^2)^2-\Omega_0^2 f^2\right). \tag{17}$$

Using the Lagrangian, one finds that field configurations that satisfy the equations of motion also satisfy

$$\frac{dL}{d\omega} = Q, \tag{18}$$

as in flat space. A straightforward calculation produces

$$\frac{dE}{d\omega} = Q + \omega\frac{dQ}{d\omega} - \frac{dL}{d\omega} = \omega\frac{dQ}{d\omega}, \tag{19}$$

implying that

$$\frac{dE}{dQ} = \omega. \tag{20}$$

We emphasize that, although we have chosen a specific potential, this differential relation relating the energy and charge holds for all potentials. This result also gives ω a simple interpretation as a chemical potential, describing how the energy changes as the particle number changes.

III. THIN-WALL Q-BALLS

Following Coleman [13], we can treat Eq. (14) as describing a particle rolling in a potential $V(f,\rho)$ defined as

$$V(f,\rho) = \frac{f^2}{2(1+\rho^2/\lambda^2)}\left[\frac{\Omega^2}{1+\rho^2/\lambda^2}-\Omega_0^2-(1-f^2)^2\right], \tag{21}$$

where the ρ coordinate is treated as an effective time. Since the potential depends on ρ, the physics is of a particle rolling in a time-dependent potential. In flat space and AdS, the coefficient of the f' term decreases with increasing ρ, which is interpreted as a friction that decreases with time. In flat space, thin-wall trajectories are those in which the particle starts rolling from rest near a maximum in the potential but does not complete the large field change, rolling down the hill, until the friction term has become somewhat small. This leads to a fast transition, or a thin wall for the soliton. All of the Q-ball trajectories end at $f = 0$ to ensure a field configuration that is localized in space.

An example of thin-wall Q-balls in AdS, where the field stays at the false minimum of U at $f = f_+$ for a long time before making a quick transition to the true minimum of U at $f = 0$, is shown in Fig. 1. The left panel shows the Q-ball profile found numerically using collocation algorithms implemented by SciPy [23]. In the right panel, we show the effective potential $V(f,\rho)$ as a function of f for several values of ρ. The field value at a specific value of ρ is shown as a dot.

The effective potential is found to have extrema at $f = 0$ and

$$f_\pm^2 \equiv \frac{2}{3}\pm\frac{1}{3}\sqrt{1+\frac{3\Omega^2}{1+\rho^2/\lambda^2}-3\Omega_0^2}. \tag{22}$$

We note that f_+ can take real values, while f_- does not when

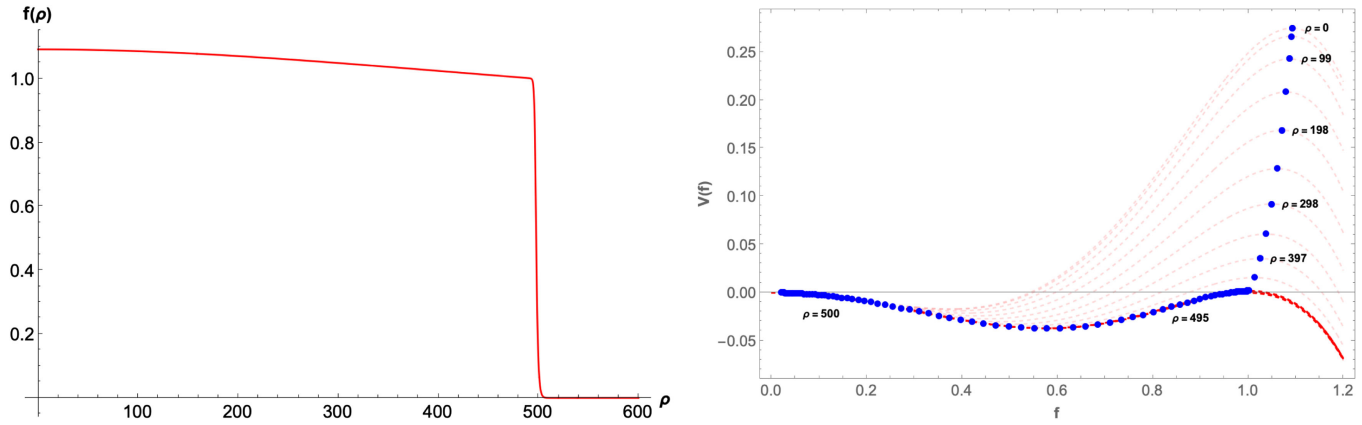

FIG. 1. Left: numerical Q-ball profile in solid red for $\lambda = 500$ and $\Omega_0 = 1/\sqrt{2}$, $\Omega = 0.99$. Right: effective potential in dashed red $V(f,\rho)$ for the same parameters and various values of ρ, where the blue dots indicate the location of the field value.

$$\Omega^2 \geq \left(1 + \frac{\rho^2}{\lambda^2}\right)(1 + \Omega_0^2). \tag{23}$$

Within these restrictions, we find that f_+ corresponds to a maximum and f_- to a minimum. A more restrictive constraint on Q-ball profiles is that if the "particle" is to roll down a slope that ends at the f_+ maximum, then that maximum must have positive energy, or $V(f,\rho) > 0$, for the particle trajectory to overcome the residual friction and end at $f = 0$. However, we find that $V(f_+(\rho),\rho) = 0$ for

$$\rho^2 = \lambda^2 \frac{\Omega^2 - \Omega_0^2}{\Omega_0^2}. \tag{24}$$

Trajectories that have not already rolled to near the $f = 0$ maximum by this value of ρ cannot produce a localized soliton configuration. This limits the radius of thin-wall AdS Q-balls to

$$R_{\text{thin-wall}} \lesssim \lambda \frac{\sqrt{\Omega^2 - \Omega_0^2}}{\Omega_0}. \tag{25}$$

For flat-space Q-balls, the extremum at $f = 0$ is always a maximum because $\Omega^2 - \Omega_0^2 < 1$ for Q-ball configurations. In an AdS background (as we will see below), this restriction does not apply. Thus, we find that

$$\left.\frac{d^2V}{df^2}\right|_{f=0} = \frac{\Omega^2 - (1 + \rho^2/\lambda^2)(1 + \Omega_0^2)}{(1 + \rho^2/\lambda^2)^2} \tag{26}$$

can lead to a minimum at $f = 0$, at least until ρ becomes sufficiently large. Note that this is exactly the same condition for the minimum at f_- to not exist. In this case, the maximum at f_+ rolls directly to the minimum at $f = 0$. This behavior gives rise to a class of AdS Q-balls with no flat-space analogue.

We take the large field transition to occur at $\rho = R \gg 1$. This implies that for $\rho \ll R$, we should take the solution to be approximately $f = f_+(\rho)$. This is not an exact solution to the equations because the derivatives of $f_+(\rho)$ are nonzero, but f'_+/f_+ is of order $\frac{1}{\lambda}$, so for $\lambda \gg 1$ the corrections to this solution are small.

On the other hand, when $\rho \sim R$ the field transitions between the two vacua and the derivatives are not small. To analyze this region, we define an energy-like quantity,

$$W = \frac{1}{2}f'^2 + V(f,\rho), \tag{27}$$

to analyze the transition region of the Q-ball. For a thin-wall transition, we expect this "energy" to be approximately conserved, so W is constant. Note that as $\rho \to \infty$, $W \to 0$ because the particle comes to rest at $V(0,\infty) = 0$. In this approximation, we can neglect the contributions to f' away from the radius of the soliton, which we define by $f''(R) = 0$. The equation is then

$$\frac{df}{d\rho} = \sqrt{-2V(f,R)} = \frac{f}{\sqrt{1 + R^2/\lambda^2}}\sqrt{(1 - f^2)^2 - \frac{\Omega^2}{1 + R^2/\lambda^2} + \Omega_0^2}. \tag{28}$$

Finally, we expect this equation to be most correct when the particle rolls with the least amount of friction. This would be for cases that come as close as possible to saturating the bound in Eq. (25). In this case, the differential equation is

$$\frac{df}{d\rho} = \frac{f}{\sqrt{1 + R^2/\lambda^2}}(1 - f^2), \tag{29}$$

which leads to the transition profile

$$f_t(\rho) = \frac{1}{\sqrt{1 + 2e^{2(\rho - R)/\sqrt{1 + R^2/\lambda^2}}}}. \tag{30}$$

To match the interior solution, we multiply by $f_+(\rho)$, so our approximate thin-wall profile is

$$f_T(\rho) = \frac{f_+(\rho)}{\sqrt{1+2e^{2(\rho-R)/\sqrt{1+R^2/\lambda^2}}}}. \tag{31}$$

This transition function allows us to capture the leading-order effects of friction of the particle trajectories. Using the equations of motion for f, we find

$$\frac{dW}{d\rho} = -\frac{2}{\rho}\frac{1+2\rho^2/\lambda^2}{1+\rho^2/\lambda^2}f'^2 + \frac{\rho f^2}{\lambda^2(1+\rho^2/\lambda^2)^2}\left[\Omega_0^2 - \frac{2\Omega^2}{1+\rho^2/\lambda^2} + (1-f^2)^2\right]. \tag{32}$$

By integrating from $\rho = R - z_0$ to $\rho = \infty$, we find

$$W_\infty - W_{R-z_0} = -2\int_{R-z_0}^{\infty}\frac{d\rho}{\rho}\frac{1+2\rho^2/\lambda^2}{1+\rho^2/\lambda^2}f'^2 + \int_{R-z_0}^{\infty}d\rho\frac{\rho f^2}{\lambda^2(1+\rho^2/\lambda^2)^2} \times\left[\Omega_0^2 - \frac{2\Omega^2}{1+\rho^2/\lambda^2} + (1-f^2)^2\right]. \tag{33}$$

We find the leading effect from the friction by evaluating these integrals using the transition function defined in Eq. (31), similar to the analysis done in [14]. Equation (33) then yields the relation

$$\Omega_0^2 - \frac{\Omega^2}{1+\frac{R^2}{\lambda^2}} = \frac{\lambda^2R^2(\Omega^2\ln 4 - 5) - 2\lambda^4 - 3R^4}{2R\lambda(\lambda^2+R^2)^{3/2}}. \tag{34}$$

This relation for a more general n-dimensional AdS background is derived in more detail in the Appendix.

IV. NUMERICS

We begin by verifying that our analytic understanding of Q-balls in AdS agrees with numerical solutions. Solutions to the profile equation (14) are obtained numerically through the use of SciPy [23]. We consider two benchmark points, corresponding to (a) $\lambda = 500$, $\Omega_0 = 1/\sqrt{2}$ and (b) $\lambda = 100$, $\Omega_0 = 1/10$. For each benchmark point, solutions are generated for various choices of Ω.

Figure 2 shows the comparison between the numerical calculations (red dashed) and analytic predictions (blue) for the benchmark point $\lambda = 500$, $\Omega_0 = 1/\sqrt{2}$. The left panel shows the obtained numeric values for the Q-ball radius R as a function of ω with a comparison to the analytic predictions from Eq. (34). The difference between the numerical and analytical results is negligible. The vertical dashed line is $\omega = m_\phi$ or $\Omega = \sqrt{1+\Omega_0^2}$. In flat space, there are no Q-ball solutions beyond this point, but we find both numerical and theoretical evidence for these solitons in AdS space. The red dot indicates the $E = mQ$ instability point, which is described below. Soliton solutions to the right of this point on the curve are unstable to dissociation.

The right panel of Fig. 2 compares the numerical and analytic predictions [as predicted by (31)] for the two Q-ball profiles for the same parameters $\lambda = 500$, $\Omega_0 = 1/\sqrt{2}$, and $\Omega = 0.99$. The two different solutions for R lead to two different profile functions of very different radius. Once again, the difference between the numerical and analytical results is negligible for both profiles.

Figure 3 is similar to Fig. 2, except that the benchmark point is $\lambda = 100$, $\Omega_0 = 1/10$. As with the previous plot, the difference between the numeric and analytic results regarding the radius of the Q-balls is completely negligible. It is in principle possible to modify our radius prediction to obtain better accuracy for even larger AdS curvature. Any miscalculation of the radius feeds into the profile prediction and, in fact, is the largest source of error for near thin-wall profiles. As seen in the right panel of Fig. 3, when we

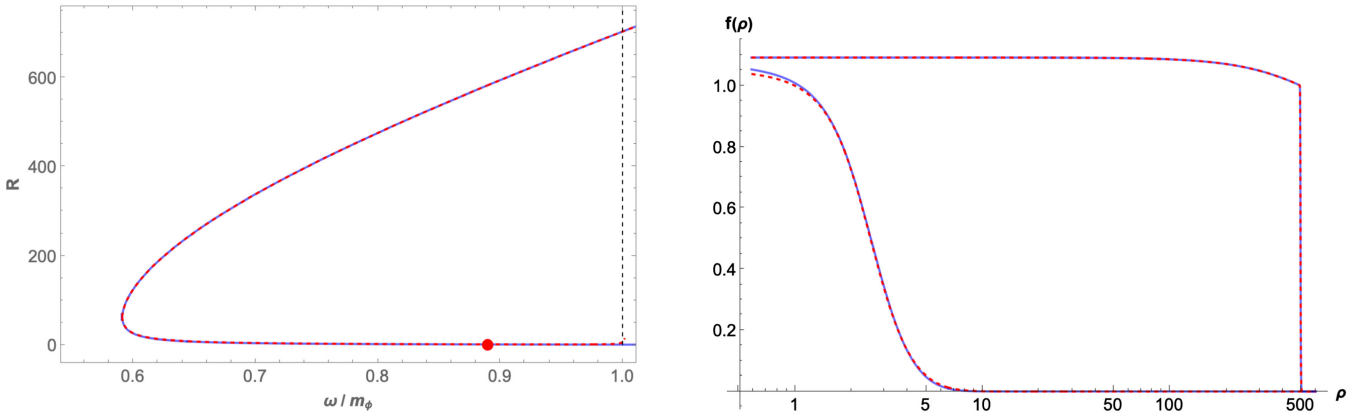

FIG. 2. Numerical calculations (red dashed) compared to analytic predictions (blue) for $\lambda = 500$, $\Omega_0 = 1/\sqrt{2}$. Left: Q-ball radius R as a function of ω. Right: both Q-ball profiles for $\Omega = 0.99$.

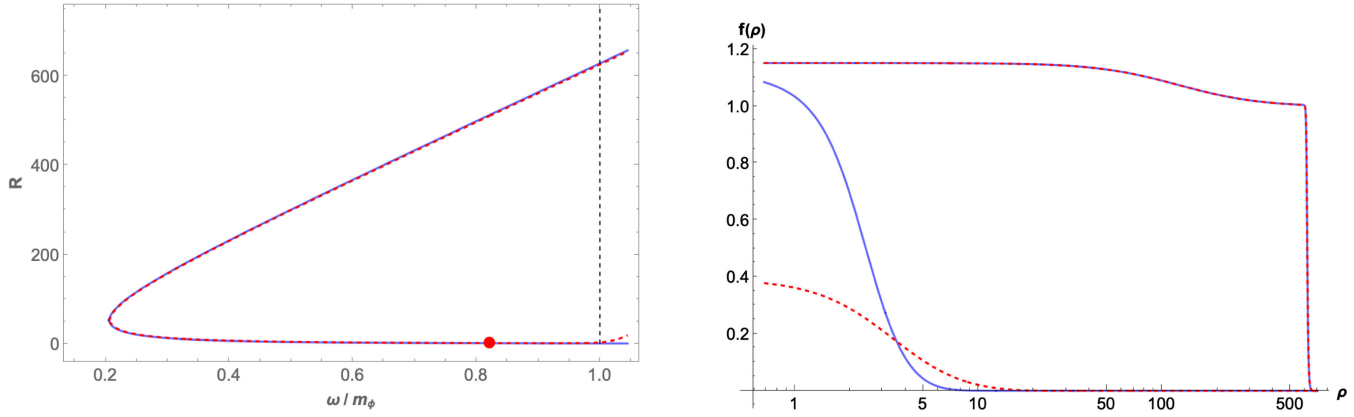

FIG. 3. As in Fig. 2, but for the benchmark point $\lambda = 100$, $\Omega_0 = 1/10$. Red dashed curves are numerical results and blue curves are the analytic predictions.

correct for the radius the functional form of the analytic thin-wall profile remains impressively accurate. The profiles with smaller radii are not fit well by our analytic profile. This is because our calculation assumed that the particle begins rolling from the maximum of the potential, but for these profiles the particle begins rolling some way downhill of the maximum.

As can be seen, there is overall an excellent match between the analytical predictions from the previous section and the numerical results near the thin-wall limit. Away from the thin-wall limit, the analytic approximations do not provide a good fit to the profile. It is likely that this fit could be improved by making a more careful analysis of profiles that do not begin near the maximum of the potential.

In Fig. 4 we plot the predicted (solid) and numerical (dashed) radius for AdS Q-balls for $\lambda = 500$ (black), 100 (read), and 10 (blue). A few general characteristics of the solution space are evident. For larger and larger λ, we approach the flat-space limit, in which the upper branch of solutions is pushed to infinite radius. As λ increases, the value of ω at which the upper branch begins becomes larger, leading to a smaller radius at which $\omega = m_\phi$. We also see that the lower-branch Q-balls near $\omega = m_\phi$ with increasing radius are seemingly pulled out of the solution space as λ increases.

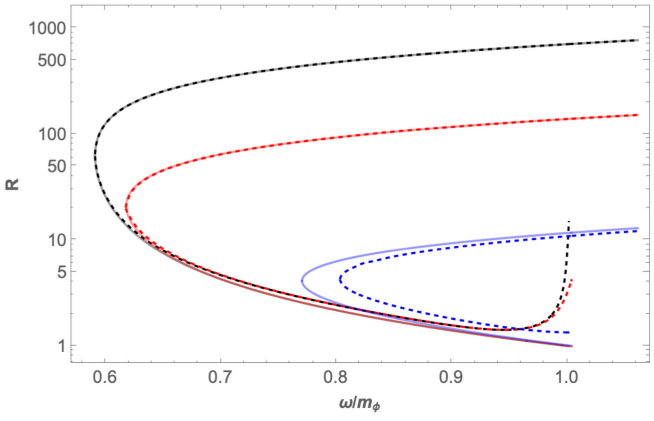

FIG. 4. Plot of radius vs ω/m_ϕ for $\lambda = 500$ (black), 100 (red), and 10 (blue). The theoretical predictions for the radius are shown as solid lines, while the numerical data are show as dashed lines.

These observations are quite similar to what has been demonstrated for gauged Q-balls in flat space [24]. In that case, increasing the gauge coupling has a similar effect to increasing λ [25]. This can be understood by the mapping of global Q-balls into the gauged Q-ball solution space [15,17], which suggests that, even though flat-space gauged Q-balls differ significantly from global AdS Q-balls, a similar mapping from the flat-space global solution to the global AdS solution space can also be defined.

We emphasize that from the figures, unlike in flat space [13], there are AdS Q-balls for $\omega > m_\phi$. We have shown this for the three benchmarks in Fig. 4, but it seems to apply quite generally. As discussed in the previous section, in the full profile equation (14), the term proportional to Ω is itself suppressed at large ρ, and so we can have solutions that are localized, even if $\omega > m_\phi$. This might appear to suggest that these AdS Q-balls have an arbitrarily large radius. The following sections, however, argue that this is not the case.

V. INSTABILITIES

In this section, we discuss two different instabilities related to global Q-balls. The first is familiar from flat-space solitons, but the second is new to the AdS case.

There exist solutions to the field equation with $E/Q > m_\phi$ and $\frac{dE}{dQ} < m_\phi$, where E is the energy and Q is the global charge, for both flat-space and AdS Q-balls. At these points in parameter space, a Q-ball is unstable to dissociation into Q individual, independent particles of mass m_ϕ. The emission of just a few particles does not stabilize the soliton because $\frac{dE}{dQ} = \omega < m_\phi$, so shedding individual charged particles makes E/Q even larger. Therefore, any soliton of this type completely falls apart. Thus, the lowest-energy

state with this charge is expected to be a gas of free particles without any soliton contribution.

However, in AdS (but not in flat space) we can have $\frac{dE}{dQ} > m_\phi$. In this case, removing a particle from the Q-ball decreases the energy of the system, as the energy required to remove the particle is more than compensated by the binding energy. Such a Q-ball will therefore radiate particles until it reaches a state with $\frac{dE}{dQ} = m_\phi$, with an additional gas of free particles of mass m_ϕ. From the relation $\frac{dE}{dQ} = \omega$, we find that if for a global charge Q the Q-ball solution has $\omega < m_\phi$, it remains a pure Q-ball solution. Conversely, if for a fixed charge Q the soliton solution has $\omega > m_\phi$, it sheds particles, leading to a field configuration with a Q-ball plus additional unbound particles.

These instability points are marked for the benchmark points in Figs. 2 and 3. The red dot indicates the point at which $E = m_\phi Q$; to the right of this point, the lower branch becomes unstable to a state completely composed of free particles. We also show the line $\omega = m_\phi$. To the right of this line, we have $\frac{dE}{dQ} > m_\phi$ and the upper branch becomes unstable to a soliton of smaller charge surrounded by a gas of free particles.

The implication is that in AdS, generically, there is 1) a minimum charge $Q_{\min}$ for Q-balls below which $E = m_\phi Q$ and the soliton dissolves into particles, 2) a maximum charge $Q_{\max}$ for Q-balls where $\omega = m_\phi$ and beyond which a gas of particles forms around the Q-ball, and 3) the two branches of solutions as functions of ω that show that there is a charge Q where the frequency ω is minimized to some value $\omega_{\min}$.

In Fig. 5 we illustrate the phase diagram of AdS Q-balls as a function of the total charge Q and ω_0 for the benchmark value of $\lambda = 100$. The phase of a free gas of unbound particles is largely the same as for flat-space Q-balls. However, the phase on the right of the diagram cannot occur in flat space.

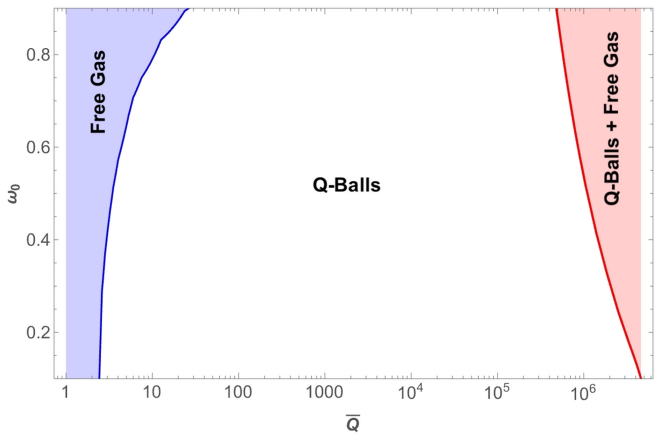

FIG. 5. Phase diagram of the theory as a function of ω_0 and the total charge $\bar{Q} \equiv Q/4\pi\phi_0^2$ for $\lambda = 100$. The phase on the right (red) appears for Q-balls in the AdS background, but not in flat space.

VI. COMMENTS ON LARGE RADIUS AdS Q-BALLS

It is interesting to note that in AdS space the thin-wall Q-balls must have a maximal radius. This is easily seen by using the language of a particle rolling in a potential. In the thin-wall approximation, the field stays at the second maximum until it transitions. However, for extremely large R, the energy of the second maximum drops below the energy at $f = 0$ and the transition can no longer occur. Therefore, there is a maximum possible radius.

There are two possible avenues to having stable AdS Q-balls with large radii. First, one could consider non-thin-wall solutions where the Q-ball profile rolls slowly between the two maxima. These solutions cannot be treated analytically using our methods, and so the formula (34) does not apply. However, the general argument of the previous paragraph still applies; as ρ increases, the entire potential drops, and eventually the field does not have the energy to return to the final field value at $f = 0$.

The other possibility is to consider an entirely different class of potential. The effective potential for the particle is of the form

$$V(f,\rho) = \frac{\Omega^2 f^2}{(1+\frac{\rho^2}{\lambda^2})^2} - \frac{U(f)}{1+\frac{\rho^2}{\lambda^2}}. \tag{35}$$

For large ρ, the first term is additionally suppressed, and in our case we recover similar dynamics to the original sextic potential, where the second maximum is below the maximum at $f = 0$. However, we can consider a potential where the first term is always dominant at large f; this can happen if $U(f)$ grows slower than f^2 at large f. An example is the exponential potential considered in [19], where the potential goes to a constant at large f. In this model, the authors of [19] indeed found Q-balls of arbitrarily large radius and charge. We therefore find that the existence of large Q-balls in AdS is possible, but it requires a specific form of potential. We leave this issue for future consideration.

VII. IMPLICATIONS IN THE DUAL THEORY

From the AdS/CFT correspondence, we expect our results to have an interpretation in a dual three-dimensional field theory. While the precise nature of this field theory is not determined, we note that the scalar field in the AdS bulk must map to a scalar field operator in the dual boundary theory. This operator is typically a composite of the fundamental fields of the theory. We leave the nature of the fundamental theory unspecified, but we assume that it has a low-energy limit or sector that is dominated by the interactions of this scalar operator. One intriguing possibility is that the AdS Q-balls are dual to scar states [26,27].

These states have been tied to nontopological AdS soliton states without horizons [28], such as boson stars and oscillons, though the connection to Q-balls has not been established. In any case, the bulk potential determines certain properties of the scalar operator and, in particular, the dimension of this operator is [1]

$$\Delta = \frac{d}{2} + \sqrt{\frac{d^2}{4} + \ell^2 m_\phi^2}, \tag{36}$$

where d is the dimension of the space and ℓ is the AdS radius.

The charge of the $U(1)$ scalar field in AdS maps to a $U(1)$ charge on the boundary. More precisely, by weakly gauging the $U(1)$ global symmetry of bulk theory (so that the gauge field does not affect the structure of the Q-ball), this symmetry would be dual to a global $U(1)$ symmetry on the boundary. By construction, the scalar field operator on the boundary carries a charge under this global $U(1)$, and states created by the action of this operator also carry this global charge.

We can understand the dynamics of this sector and, in particular, the structure of the ground state of the theory as a function of the charge Q by using the bulk Q-ball solution.

Small charge: From the bulk description, we see that for very small charges, the solution is a gas of free particles. The energy increases proportionally to Q as $E = m_\phi Q$ [here m_ϕ is related to the operator dimension by (36)].

Intermediate charge: As we increase the charge, there is a critical value (corresponding to $Q_{\min}$) at which the ground state becomes a condensate carrying charge Q. The Q-ball is localized in the interior of the AdS space and has a nontrivial dependence on the r coordinate. This indicates that the three-dimensional field theory condensate has a nontrivial dependence on scale.

At the transition point, the condensate has an energy $E = m_\phi Q$. Therefore, the transition does not lead to a discontinuous jump in the energy. However, the condensate has an energy dependence of the form $\frac{dE}{dQ} = \omega$, in contrast to the free gas, which has the relation $\frac{dE}{dQ} = m_\phi$. Since the transition occurs at a value of ω that is not equal to m_ϕ (as seen in Figs. 2 and 3), we see that there is a discontinuity in $\frac{dE}{dQ}$. This is therefore a second-order phase transition. As the charge increases further, the condensate becomes increasingly bound until the binding energy per particle reaches a maximum value of $m_\phi - \omega_{\min}$.

Large charge: As we continue to increase the charge, the binding energy begins to decrease and vanishes at $Q_{\max}$. Beyond this point, additional charge is not absorbed into the condensate. However, the condensate does not evaporate; instead, the condensate is surrounded by a gas of free particles. More precisely, the condensate carries a charge $Q_{\max}$, and the remaining charge $Q - Q_{\max}$ is in free particles.

As mentioned above, the condensate has an energy dependence of the form $\frac{dE}{dQ} = \omega$. Since the transition occurs exactly at $\omega = m_\phi$, the energy dependence is $\frac{dE}{dQ} = m_\phi$. This is equal to the change in energy when we add a free particle. This implies that $\frac{dE}{dQ}$ is continuous. However, for the gas around the Q-ball, $\frac{d^2E}{dQ^2} = 0$, while for the Q-ball, $\frac{d^2E}{dQ^2} = \frac{d\omega}{dQ}$. Hence, $\frac{d^2E}{dQ^2}$ is discontinuous, which implies that this is a *third-order* phase transition.

VIII. Q-BALLS IN n-DIMENSIONAL AdS

The above analysis has assumed a $3+1$ AdS space, which maps to a $2+1$ conformal field theory (CFT). In this section, we outline how our results generalize to $(n-1)+1$ AdS spaces related to $(n-2)+1$ CFTs. The AdS geometry in n dimensions is parametrized as

$$ds^2 = a(r)dt^2 - b(r)dr^2 - r^2 d\Omega_{n-2}^2, \tag{37}$$

with

$$a(r) = 1 + \frac{r^2}{\ell_n^2}, \qquad b(r) = \frac{1}{1 + \frac{r^2}{\ell_n^2}}, \tag{38}$$

where $\ell_n = \sqrt{-\frac{(n-2)(n-1)}{\Lambda}}$ and $d\Omega_{n-2}^2$ is the measure on the $(n-2)$-sphere. Assuming a spherically symmetric solution, as before, the action becomes

$$\mathcal{S} = S_{n-2}\phi_0^2 \int dt dr r^{(n-2)} \left[\frac{1}{2}\frac{\omega^2 f^2}{1 + r^2/\ell_n^2} - \frac{1}{2} f'^2 (1 + r^2/\ell_n^2) - \bar{U}(\phi_0^2 f^2/2)\right], \tag{39}$$

where

$$\bar{U} = \frac{1}{2}(m_\phi^2 - \omega_0^2) f^2 (1 - f^2)^2 + \frac{\omega_0^2}{2} f^2. \tag{40}$$

We can then consider f to be a particle rolling in a time-dependent potential, as before, with the Lagrangian

$$L = r^{(n-2)} \left[\frac{1}{2}\frac{\omega^2 f^2}{1 + r^2/\ell_n^2} - \frac{1}{2} f'^2 (1 + r^2/\ell_n^2) - \frac{1}{2}(m_\phi^2 - \omega_0^2) f^2 (1 - f^2)^2 - \frac{\omega_0^2}{2} f^2\right]. \tag{41}$$

Transforming to dimensionless parameters ρ, Ω, Ω_0, and $\lambda_n = \ell_n \sqrt{m_\phi^2 - \omega_0^2}$, the Lagrangian can be written as

$$L = \frac{\rho^{(n-2)}}{(m_\phi^2-\omega_0^2)^{n-3}}\left[\frac{1}{2}\frac{\Omega^2 f^2}{1+\rho^2/\lambda_n^2} - \frac{1}{2}(f')^2(1+\rho^2/\lambda_n^2) - \frac{1}{2}f^2(1-f^2)^2 - \frac{\Omega_0^2}{2}f^2\right]. \tag{42}$$

The equation of motion for $f(\rho)$ is

$$f'' + \frac{n-2}{\rho}\frac{1+(\frac{n}{n-2})(\rho^2/\lambda_n^2)}{1+\rho^2/\lambda_n^2}f' = \frac{f}{1+\rho^2/\lambda_n^2}\left[1+\Omega_0^2 - \frac{\Omega^2}{1+\rho^2/\lambda_n^2} - 4f^2 + 3f^4\right] \equiv -\frac{\partial V}{\partial f}, \tag{43}$$

where $V(f,\rho)$ is the effective potential, given explicitly by

$$V(f,\rho) = \frac{f^2}{2(1+\rho^2/\lambda_n^2)}\left[\frac{\Omega^2}{1+\rho^2/\lambda_n^2} - \Omega_0^2 - (1-f^2)^2\right] \tag{44}$$

after imposing $V(0,\infty)=0$. The effective potential is unchanged from the $n=4$ case aside from the substitution $\lambda \to \lambda_n$. Defining the energy-like quantity W as in Eq. (27), we find that W is approximately conserved for the thin-wall solutions and the approximate thin-wall profile for the n-dimensional case is then given by

$$f_{T,n}(\rho) = \frac{f_{+,n}(\rho)}{\sqrt{1+2e^{2(\rho-R)/\sqrt{1+R^2/\lambda_n^2}}}}, \tag{45}$$

with

$$f_{+,n}(\rho) \equiv \frac{2}{3} + \frac{1}{3}\sqrt{1+\frac{3\Omega^2}{1+\rho^2/\lambda_n^2} - 3\Omega_0^2}. \tag{46}$$

Using the equations of motion for f [Eq. (43)], we find

$$\frac{dW}{d\rho} = -\frac{(n-2)}{\rho}\frac{1+(\frac{n}{n-2})\rho^2/\lambda_n^2}{1+\rho^2/\lambda_n^2}f'^2 + \frac{\rho f^2}{\lambda_n^2(1+\rho^2/\lambda_n^2)^2}\left[\Omega_0^2 - \frac{2\Omega^2}{1+\rho^2/\lambda_n^2} + (1-f^2)^2\right]. \tag{47}$$

By integrating from $\rho = R - z_0$ to $\rho = \infty$, we find

$$W_\infty - W_{R-z_0} = -(n-2)\int_{R-z_0}^{\infty}\frac{d\rho}{\rho}\frac{1+(\frac{n}{n-2})\rho^2/\lambda_n^2}{1+\rho^2/\lambda_n^2}f'^2 + \int_{R-z_0}^{\infty}d\rho\frac{\rho f^2}{\lambda_n^2(1+\rho^2/\lambda_n^2)^2}\left[\Omega_0^2 - \frac{2\Omega^2}{1+\rho^2/\lambda_n^2} + (1-f^2)^2\right]. \tag{48}$$

Once again, we compute the leading-order effect of the friction by evaluating these integrals using the transition function defined in Eq. (45), which results in the relation

$$\Omega_0^2 - \frac{\Omega^2}{1+\frac{R^2}{\lambda_n^2}} = \frac{\lambda_n^2 R^2(\Omega^2\ln(4) - 2n + 3) - (n-2)\lambda_n^4 - (n-1)R^4}{2R\lambda_n(\lambda_n^2+R^2)^{3/2}}. \tag{49}$$

This relation is derived in more detail in the Appendix. Note that this relation exactly matches the previous implicit equation for R [Eq. (34)] for $n=4$. Figure 6 shows the numerical and predicted Q-ball radius as a function of ω for $n=3$ and $n=5$, with $\lambda_n = 500$ and $\Omega_0 = 1/\sqrt{2}$ for both cases. These results show that AdS Q-balls can be constructed in various dimensions using these methods. Consequently, the qualitative analysis of their dual CFTs follows, including similar-looking phase diagrams to those shown in the previous section.

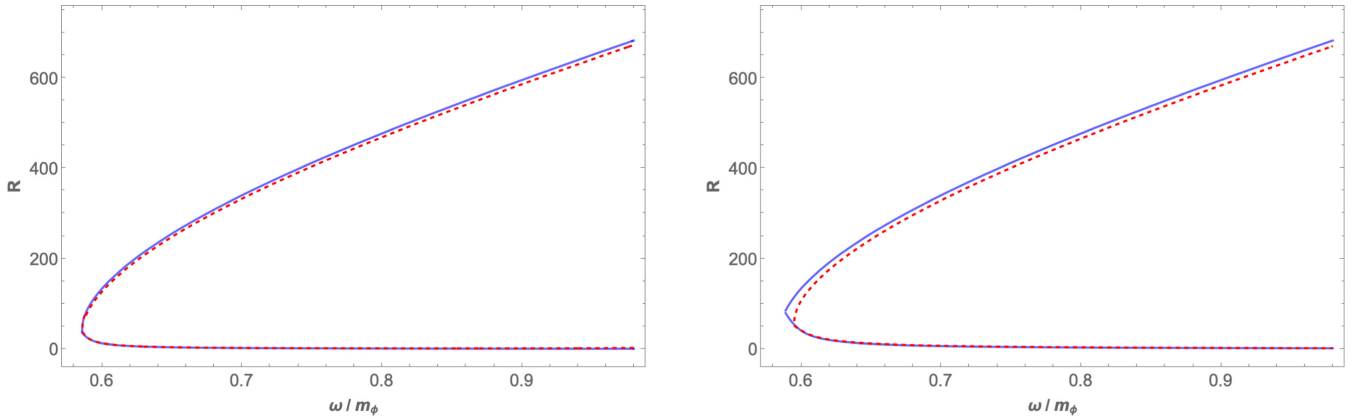

FIG. 6. Numerical calculations (red dashed) compared to analytic predictions (blue) for $\lambda_n = 500$, $\Omega_0 = 1/\sqrt{2}$. Left: Q-ball radius R as a function of ω for $n=3$. Right: Q-ball radius R as a function of ω for $n=5$.

IX. DISCUSSION AND CONCLUSION

In this article, we have studied Q-balls in a fixed AdS background, with particular focus on thin-wall Q-balls. The scalar field is subject to a sextic potential (which also supports Q-balls in a flat background), but the general features are expected to apply to most (if not all) potentials that support thin-wall solitons. We have shown that the AdS background significantly modifies the physics of these Q-balls, even if gravity is not dynamical. In particular, Q-balls have a maximal radius in AdS, unless the potential is of a very special type.

We have also found new phases of the scalar field that composes the Q-balls that do not exist in flat space. Specifically, for large charges, the lowest-energy field configuration is a Q-ball surrounded by a gas of massive particles, while in flat space the ground state for larger charge is just a Q-ball with larger mass and radius.

The transitions between the states are also of a novel type. At low charges, as the charge is increased, there is a zero-temperature second-order phase transition to a Q-ball state, similar to flat-space systems. Curiously, at high charges, there is a *third*-order phase transition to the mixed Q-ball scalar gas state mentioned above. This phase transition has no flat-space analogue. These results imply that the dual boundary theory must also have similar transitions. It would be quite interesting to explore whether scar states, similar to those related to other nontopological solitons in AdS, can be related to AdS Q-balls. If so, one should be able to understand this third-order phase transition in the context of scar states.

In this work we have ignored backreaction on the geometry. This implies that the gravitational interactions of order $\frac{1}{M_{\rm pl}}$ have been dropped, while keeping the curvature scale of the AdS constant. In terms of the original AdS/CFT correspondence, this amounts to taking the N of the dual gauge group to infinity while keeping the 't Hooft coupling g^2N fixed.

Including dynamical gravity on the AdS side would be an important next step to see if these novel phase transitions survive the inclusion of gravity. It would also be interesting to connect these solutions to the known boson star solutions. Finally, there is cosmological motivation to extend these solutions to a full characterization of Q-balls in de Sitter space [29]. We leave these and other questions for future work.

ACKNOWLEDGMENTS

We thank Julian Heeck for helpful comments on various aspects of this work. The work of A. R. is supported by the National Science Foundation Grant No. PHY-1915005. C. B. V. is supported in part by the National Science Foundation under Grant No. PHY-2210067.

APPENDIX: DERIVATION OF Q-BALL RADIUS FORMULA

In order to derive Eq. (49), we must evaluate

$$W_\infty - W_{R-z_0} = -(n-2)\int_{R-z_0}^{\infty}\frac{d\rho}{\rho}\frac{1+(\frac{n}{n-2})\rho^2/\lambda_n^2}{1+\rho^2/\lambda_n^2}f'^2 + \int_{R-z_0}^{\infty}d\rho\frac{\rho f^2}{\lambda_n^2(1+\rho^2/\lambda_n^2)^2}\left[\Omega_0^2-\frac{2\Omega^2}{1+\rho^2/\lambda_n^2} + (1-f^2)^2\right]. \tag{A1}$$

We assume that $R \gg \lambda_n$. The first integral on the right-hand side can be approximated by noting that the dominant contribution occurs about the transition between minima at $\rho = R$. We define the function $f_{t,n}(\rho)$ as

$$f_{t,n}(\rho) = \frac{1}{\sqrt{1+2e^{2(\rho-R)/\sqrt{1+R^2/\lambda_n^2}}}}, \tag{A2}$$

so that $f(\rho) = f_{+,n}(\rho)f_{t,n}(\rho)$. Around $\rho = R$, we have $f'(\rho) \approx f_{+,n}(\rho)f'_{t,n}(\rho)$. Since the integrand is exponentially suppressed below $\rho = R$, we can integrate from $\rho = 0$ to ∞ rather than from $R - z_0$ to ∞. This integral can be performed analytically, and after dropping another exponentially suppressed term in the result it yields

$$(n-2)\int_{R-z_0}^{\infty}\frac{d\rho}{\rho}\frac{1+(\frac{n}{n-2})\rho^2/\lambda_n^2}{1+\rho^2/\lambda_n^2}f'^2 \approx -\frac{\lambda_n(\lambda_n^2(n-2)+nR^2)\left(2+\sqrt{1+\frac{3\lambda_n^2\Omega^2}{\lambda_n^2+R^2}-3\Omega_0^2}\right)}{12R(\lambda_n^2+R^2)^{3/2}}. \tag{A3}$$

The second integral in Eq. (A1) can be evaluated by expanding the integrand about $\rho = R$ to first order in $\rho - R$ [except for the exponential piece in $f_{t,n}(\rho)$ since its series expansion does not converge; however, we will still be able to do these integrals analytically while including this exponential piece]. The resulting expression will be very large and have a dependence on z, but this dependence will match exactly with the z dependence on the left-hand side of Eq. (A1) and cancel out.

On the left-hand side, we need to expand $W(\rho)$, given by Eq. (27), about $\rho = R - z$; the W_∞ piece is simply zero since the profile and potential vanish at infinity. It will be convenient to instead write $\rho = R(1-a)$, where $a = z/R$, and expand about $a = 0$. Once again, we do not expand the exponential part of $f_{t,n}(\rho)$ since this does not converge, but we will find that this just leads to extra exponentially suppressed terms, which can be dropped. After doing this substitution and expansion, we can send $a \to z/R$ and then expand the resulting expression about $z = 0$. Once again,

this results in a very large expression with some z dependence.

Noting that $W_\infty = 0$, we can rewrite Eq. (A1) as

$$W_{R-z_0} - (n-2)\int_{R-z_0}^{\infty} \frac{d\rho}{\rho} \frac{1+(\frac{n}{n-2})\rho^2/\lambda_n^2}{1+\rho^2/\lambda_n^2} f'^2 + \int_{R-z_0}^{\infty} d\rho \frac{\rho f^2}{\lambda_n^2(1+\rho^2/\lambda_n^2)^2}\left[\Omega_0^2 - \frac{2\Omega^2}{1+\rho^2/\lambda_n^2} + (1-f^2)^2\right] = 0. \tag{A4}$$

Plugging in our expressions for each term and expanding in powers of z, we find that the z dependence exactly cancels out to second order. To find an implicit expression for the Q-ball radius to leading order in $1/R$, we first rewrite λ_n in terms of a new free parameter σ via $\lambda_n = \sigma R$. We then search for an equation of the form

$$\Omega_0^2 - \frac{\Omega^2}{1+\sigma^{-2}} = f_0(n,\sigma) + \frac{1}{R} f_1(n,\sigma), \tag{A5}$$

which mirrors the form of the radius relation in [14] with $1/R$ corrections. Enforcing this relation on Eq. (A4), we find

$$f_0(n,\sigma) = 0,$$
$$f_1(n,\sigma) = \frac{1+2\sigma^4 - n(1+\sigma^2)^2 + \sigma^2(3+\Omega^2\ln(4))}{2\sigma(1+\sigma^2)^{3/2}}. \tag{A6}$$

Plugging these results into Eq. (A5) and sending $\sigma \to \lambda_n/R$ reproduces Eq. (49).

[1] O. Aharony, S. S. Gubser, J. M. Maldacena, H. Ooguri, and Y. Oz, Large N field theories, string theory and gravity, Phys. Rep. **323**, 183 (2000).

[2] J. M. Maldacena, The large N limit of superconformal field theories and supergravity, Adv. Theor. Math. Phys. **2**, 231 (1998).

[3] E. Witten, Anti-de Sitter space, thermal phase transition, and confinement in gauge theories, Adv. Theor. Math. Phys. **2**, 505 (1998).

[4] D. Astefanesei and E. Radu, Boson stars with negative cosmological constant, Nucl. Phys. **B665**, 594 (2003).

[5] A. Prikas, Q stars in anti-de Sitter space-time, Gen. Relativ. Gravit. **36**, 1841 (2004).

[6] F. Nogueira, Extremal surfaces in asymptotically AdS charged boson stars backgrounds, Phys. Rev. D **87**, 106006 (2013).

[7] Y. Brihaye, B. Hartmann, and S. Tojiev, Stability of charged solitons and formation of boson stars in 5-dimensional anti-de Sitter space-time, Classical Quantum Gravity **30**, 115009 (2013).

[8] A. Buchel, S. L. Liebling, and L. Lehner, Boson stars in AdS spacetime, Phys. Rev. D **87**, 123006 (2013).

[9] O. Kichakova, J. Kunz, and E. Radu, Spinning gauged boson stars in anti-de Sitter spacetime, Phys. Lett. B **728**, 328 (2014).

[10] S. Kumar, U. Kulshreshtha, and D. S. Kulshreshtha, Charged compact boson stars and shells in the presence of a cosmological constant, Phys. Rev. D **94**, 125023 (2016).

[11] Y. Brihaye, F. Console, and B. Hartmann, Charged and radially excited boson stars (in anti-de Sitter), Phys. Rev. D **106**, 104058 (2022).

[12] S. Hu, J. T. Liu, and L. A. Pando Zayas, Charged boson stars in AdS and a zero temperature phase transition, arXiv: 1209.2378.

[13] S. R. Coleman, Q balls, Nucl. Phys. **B262**, 263 (1985); Nucl. Phys. **B269**, 744(E) (1986).

[14] J. Heeck, A. Rajaraman, R. Riley, and C. B. Verhaaren, Understanding Q-balls beyond the thin-wall limit, Phys. Rev. D **103**, 045008 (2021).

[15] J. Heeck, A. Rajaraman, R. Riley, and C. B. Verhaaren, Mapping gauged Q-balls, Phys. Rev. D **103**, 116004 (2021).

[16] J. Heeck, A. Rajaraman, R. Riley, and C. B. Verhaaren, Proca Q-balls and Q-shells, J. High Energy Phys. 10 (2021) 103.

[17] J. Heeck, A. Rajaraman, and C. B. Verhaaren, Ubiquity of gauged Q-shells, Phys. Rev. D **104**, 016030 (2021).

[18] Y. Almumin, J. Heeck, A. Rajaraman, and C. B. Verhaaren, Excited Q-balls, Eur. Phys. J. C **82**, 801 (2022).

[19] B. Hartmann and J. Riedel, Glueball condensates as holographic duals of supersymmetric Q-balls and boson stars, Phys. Rev. D **86**, 104008 (2012).

[20] B. Hartmann, B. Kleihaus, J. Kunz, and I. Schaffer, Compact (A)dS boson stars and shells, Phys. Rev. D **88**, 124033 (2013).

[21] S. Kim, S. Kundu, E. Lee, J. Lee, S. Minwalla, and C. Patel, 'Grey Galaxies' as an endpoint of the Kerr-AdS superradiant instability, J. High Energy Phys. 11 (2023) 024.

[22] J. Heeck and M. Sokhashvili, Q-balls in polynomial potentials, Phys. Rev. D **107**, 016006 (2023).

[23] P. Virtanen *et al.* (SciPy 1.0 Contributors), SciPy1.0: Fundamental algorithms for scientific computing in Python, Nat. Methods **17**, 261 (2020).

[24] K.-M. Lee, J. A. Stein-Schabes, R. Watkins, and L. M. Widrow, Gauged Q balls, Phys. Rev. D **39**, 1665 (1989).

[25] I. E. Gulamov, E. Ya. Nugaev, A. G. Panin, and M. N. Smolyakov, Some properties of U(1) gauged Q-balls, Phys. Rev. D **92**, 045011 (2015).

[26] M. Serbyn, D. A. Abanin, and Z. Papić, Quantum many-body scars and weak breaking of ergodicity, Nat. Phys. **17**, 675 (2021).

[27] J. Cotler and A. Y. Wei, Quantum scars in quantum field theory, Phys. Rev. D **107**, 125005 (2023).

[28] A. Milekhin and N. Sukhov, All holographic systems have scar states, arXiv:2307.11348.

[29] E. Palti, P. M. Saffin, and E. J. Copeland, Dynamics of Q-balls in an expanding universe, Phys. Rev. D **70**, 083520 (2004).